Direct inelastic scattering of N_2 from Ag(111). II. Orientation

Greg O. Sitz, Andrew C. Kummel, and Richard N. Zare
Department of Chemistry, Stanford University, Stanford, California 94305

John C. Tully
AT&T Bell Laboratories, ID-346, 600 Mountain Avenue, Murray Hill, New Jersey 07974

(Received 19 April 1988; accepted 11 May 1988)

The orientation of the angular momentum of N_2 scattered from clean Ag(111) is determined by resonance-enhanced multiphoton ionization. The orientation is the net helicity or handedness of the sense of rotation, i.e., clockwise vs counterclockwise. The orientation of the scattered N_2 is measured along a direction perpendicular to the scattering plane. The degree and sign of the orientation is found to depend strongly on the final rotational quantum number J and on the final scattering angle. The results require that there are forces acting in the plane of the surface during the scattering. The observed behavior can be reproduced qualitatively by a conventional hard-cube, hard-ellipsoid model to which a tangential friction has been introduced to account for the in-plane forces. This produces a splitting of the rotational rainbow peak which leads to changes of sign of the orientation as a function of rotational quantum number. Thus, orientation measurements provide a unique probe of in-plane gas–surface forces.

I. INTRODUCTION

In general, data from scattering experiments are used to learn about the form of the potential energy surface governing the interaction. In this paper we advance the idea of measuring the orientation of the angular momentum of surface-scattered molecules as a probe of in-plane forces, i.e., that part of the potential which depends on the in-plane position of the molecule. Orientation is the net helicity or handedness of the sense of rotation of the molecule. We observe a net orientation along an axis perpendicular to the scattering plane. Since this orientation represents anisotropy in the spatial distribution of the angular momentum vector **J** projected into a plane parallel to the surface, forces in this plane are necessary to produce it.

Specifically, we report measurements of the orientation of N_2 scattered from Ag(111) determined by $2+2$ resonance-enhanced multiphoton ionization (REMPI). We observe a wide variation of the magnitude and sign of the orientation depending on final scattering angle and rotational quantum number. We complement the orientation results with alignment and population results[1,2] and correlate features between them.

This paper represents the first direct measurement of angular momentum orientation produced in scattering from a single-crystal surface. Hermans *et al.*[3] conclude from measurements of magnetic field induced changes in Knudsen flow that orientation effects are important in gas–surface interactions, but their measurements are indirect and are difficult to interpret on a microscopic level since they were done on polycrystalline gold films.

Novakoski and McClelland[4] (NM) have studied the scattering and desorption of CF_3H from Ag(111) using electrostatic focusing techniques. They found that the CF_3H is more likely to desorb with the fluorine end of the C_3 symmetry axis pointing away from the surface, and the opposite preference was found for direct scattering. Following the gas phase reactive scattering literature,[5] they use the word orientation to describe a preferential direction of the molecular axis. We employ a different meaning of the word orientation in this paper: orientation is defined to be a preferential direction of the rotational angular momentum vector of the molecule, not of the molecular axis. This is the standard definition in optical polarization experiments. Specifically, an ensemble of molecules is said to exhibit nonzero orientation about an axis x if the mean value of the angular momentum projection $\langle J_x \rangle$ is nonzero. This contrasts with the term alignment, which is a measure of the mean-square angular momentum along a direction, e.g., $\langle J_z^2 \rangle$. The orientation is the *sense* of rotation. When the molecule is viewed from a direction perpendicular to the plane of rotation, clockwise rotation of the molecule has **J** pointing away from the viewer, and counterclockwise rotation has **J** pointing toward the viewer. This type of motion is illustrated in Fig. 1 and is the main subject of this paper.

In close-coupling calculations of H_2/LiF scattering, Proctor *et al.*[6] observed a propensity for retaining orientation along z, i.e., along the surface normal $\hat{\mathbf{n}}$, whereas our measurements relate to orientation along an axis perpendicular to z. Their result reflects a conservation of M_z rather than a difference in scattering probability into final $\pm M_z$ states. Indeed, the general perception of close-packed metal surfaces as smooth and flat (based largely on He and H_2 diffraction studies) has resulted in assumptions of flat or weakly corrugated, smooth surfaces in modeling heavier particle scattering. Consequently there has been little investigation into angular momentum orientation effects in the scattering of heavy particles from close-packed surfaces.

The remainder of this paper is organized as follows: in Sec. II we briefly describe the apparatus; in Sec. III we give a more detailed discussion of the generation and use of elliptically polarized light.; in Sec. IV we present results as a function of rotational quantum number at three different final scattering angles; in Sec. V we model our results within a

 0021-9606/88/162572-11$02.10

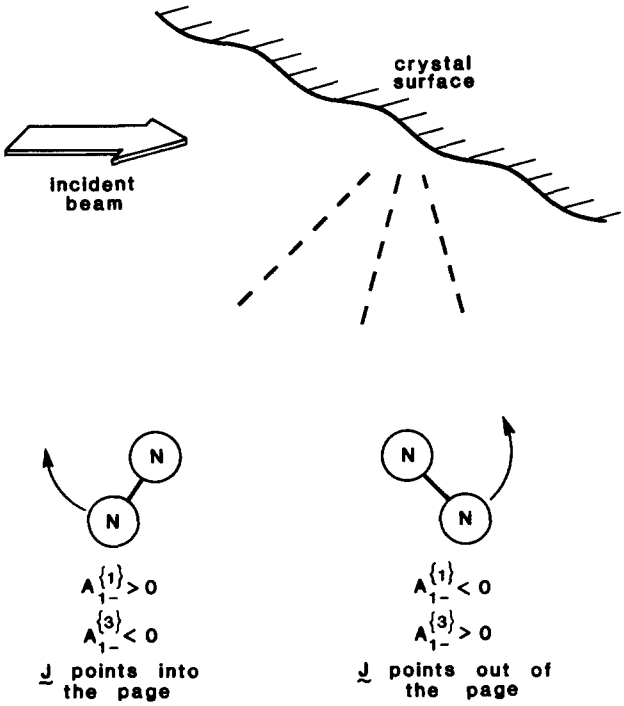

FIG. 1. Conceptual illustration of the type of angular momentum orientation measured. The plane of the paper is the scattering plane, that is, the plane containing the incident beam, the scattered beam and the surface normal. The probe laser propagates into the page and defines the orientation quantization direction. Molecules rotating clockwise have **J** pointing into the page and $A_{1-}^{\{1\}} > 0$. Those rotating counterclockwise have **J** pointing out of the page and $A_{1-}^{\{1\}} < 0$.

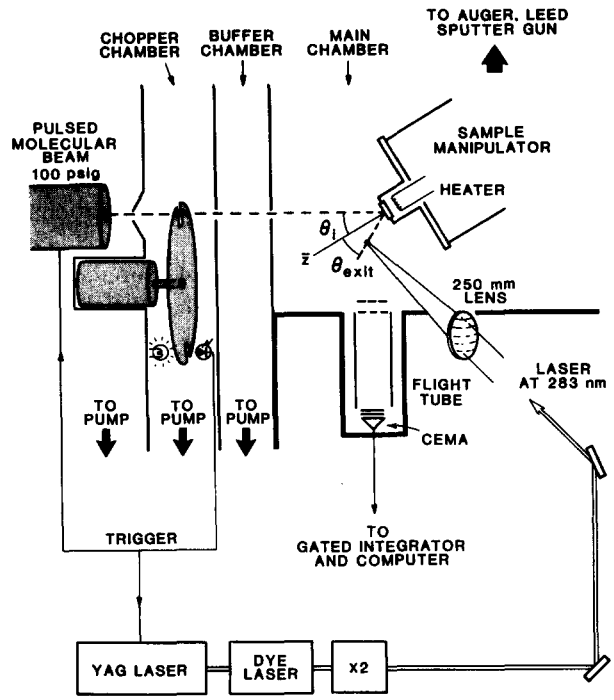

FIG. 2. Schematic diagram of the molecular beam surface scattering apparatus used in the study of the scattering of N_2 from Ag(111).

frictional hard cube model, which is shown to reproduce qualitative features of the data; and in Sec. VI we summarize our conclusions.

II. EXPERIMENTAL APPARATUS

The apparatus used in these studies is depicted schematically in Fig. 2 and has been described in detail in a previous publication.[1] Briefly, it consists of a triply differentially pumped, pulsed supersonic molecular beam source and an ultrahigh vacuum scattering chamber. All experiments reported here were done with a beam of 20% N_2 seeded in H_2 ($E_i = 0.3$ eV) incident along the [211] azimuth at 30° (measured with respect to the surface normal $\hat{\mathbf{n}}$) on the Ag(111) crystal, with the crystal temperature held at 90 K. N_2 is detected in a quantum state resolved manner by 2 + 2 resonance-enhanced multiphoton ionization as described previously. The laser beam propagates perpendicular to the plane defined by the incident beam and the surface normal, $\hat{\mathbf{n}}$. We will label the direction of the laser propagation as $-\mathbf{y}$ and the surface normal as **z**. The polarization of the laser light is controlled with half- and quarter-wave plates (Special Optics). The wave plates are zero order plates, air-spaced, and antireflection coated. The retardation was specified at 283.5 nm and was measured to be good to better than 1% across the wavelength range where experiments were done (283–285 nm).

III. ANGULAR MOMENTUM POLARIZATION MEASUREMENTS

A. Alignment

The alignment of the scattered N_2 is determined using linearly polarized light by rotating the direction of linear polarization with respect to the surface normal and recording the intensity of the REMPI signal. This has been described in detail previously,[1,2,7,8] and yields the quadrupole moment, $A_{0+}^{\{2\}}(J)$, and hexadecapole moment, $A_{0+}^{\{4\}}(J)$, of the **J** vector distribution. The moments derived in this manner are apparent moments and may include contributions from a variety of real moments. This has been discussed in detail in previous publications,[1,8] where it was argued[1] that the values of the apparent quadrupole and hexadecapole moments determined from our data are equivalent to those of the real moments within the uncertainty of the measurements.

B. Orientation

Probing orientation by two-photon excitation requires use of elliptically polarized light (as opposed to just left and right circularly polarized light) because several moments of the angular momentum distribution of the sample can contribute to the observed intensity.[8]

Elliptically polarized light is prepared by use of successive half- and quarter-wave plates. The laser is initially linearly polarized; by rotating the half-wave plate, the direction of linear polarization can be varied with respect to the optic axis of the quarter-wave plate (designated $\mathbf{z}_d$). The angle between the direction of linear polarization and the optic

axis of the quarter-wave plate will be designated β. For $\beta = 0°$, the light leaving the quarter-wave plate will remain linearly polarized, for $\beta = \pm 45°$ the light will be left/right circularly polarized and for intermediate values of β the light will be elliptically polarized with the major axis of the ellipse lying along $\mathbf{z}_d$. In our experiments $\mathbf{z}_d$ is positioned parallel to the surface normal $\mathbf{z}$. This makes calculation of the line strengths more straightforward.[8]

Experimentally, we make successive measurements of the REMPI signal for $+\beta$ and $-\beta$; this has the effect of changing the sense of rotation of the E field with respect to the laser propagation direction while keeping the ellipticity constant. It is intuitively reasonable to expect that this measurement is sensitive to the same type motion in the molecule, i.e., to the sense of rotation in a plane perpendicular to the laser propagation direction, and this is indeed the case. We make $\pm\beta$ pairs of measurements at a series of seven ellipticities between $\beta = \pm 45°$ (circular) and $\beta = 0°$ (linear). As in our previous work on alignment and population,[1] we record a short wavelength scan across a chosen transition and use the integrated area under the peak in later analysis. The laser polarization is then varied between scans.

The intensity for a two-photon transition using elliptically polarized light can be written[8]:

$$I(J_i, J_f, \beta) = n(J_i) C(\det) \{ A_{0+}^{\{0\}}(J_i, \text{apparent}) P_{0+}^{\{0\}}(J_i, J_f) + A_{1-}^{\{1\}}(J_i) P_{1-}^{\{1\}}(J_i, J_f, \beta) + A_{0+}^{\{2\}}(J_i, \text{apparent}) P_{0+}^{\{2\}}(J_i, J_f, \beta) + A_{1-}^{\{3\}}(J_i) P_{1-}^{\{3\}}(J_i, J_f, \beta) + A_{3-}^{\{3\}}(J_i) P_{3-}^{\{3\}}(J_i, J_f, \beta) + A_{0+}^{\{4\}}(J_i, \text{apparent}) P_{0+}^{\{4\}}(J_i, J_f, \beta) \}, \quad (1)$$

where $n(J_i)$ is the population of the level J_i, $C(\det)$ is a detection sensitivity constant, the $A_{q\pm}^{\{k\}}$ are the moments of the angular momentum distribution describing the spatial distribution of $\mathbf{J}$ (see below) and the $P_{q\pm}^{\{k\}}$ are the real moments of the line strength for the given transition $J_f - J_i$ for the laser polarization specified by β. The formulas for calculating the $P_{q\pm}^{\{k\}}$ are given elsewhere.[8] For two-photon excitation k ranges from 0 to 4 and q from $-k$ to $+k$. In general, two additional terms could contribute to the sum in Eq. (1), one with $k = 2$ and q odd and one with $k = 4$ and q odd. These terms were found not to be needed to fit our data. Note that the orientation terms appearing in Eq. (1) (those terms with k odd), are not apparent,[8] however, in order to facilitate comparison of moments for different J values, we reduce them by $A_{0+}^{\{0\}}$ which is apparent.

When the exciting light is linearly polarized, only terms with k even can contribute to the sum in Eq. (1). Terms with k even are used to characterize the alignment of a sample. They quantify a population difference between states with low $|J_z|$ vs high $|J_z|$, i.e., a preference for $\mathbf{J}$ to be aligned along or against a chosen axis. For elliptically polarized excitation, the restriction of k even is relaxed. Odd values of k describe orientation and represent a population difference among magnetic sublevels (in our case) with $+J_y$ vs those with $-J_y$.

The moments of the distribution are the coefficients in an expansion of the distribution

$$P(J_i, M) = n(J_i) \sum \zeta(k) A_{q\pm}^{\{k\}}(J_i) \langle J_i | J^{\{k\}} | J_i \rangle, \quad (2)$$

where $P(J_i, M)$ is the probability of being in the state $(J_i M)$, $\zeta(k)$ is a normalization constant,[8] and at high J the $\langle J_i | J^{\{k\}} | J_i \rangle$ are proportional to the real spherical harmonics $Y_{q\pm}^{\{k\}}(\theta, \phi)$. The value of each $A_{q\pm}^{\{k\}}$ then simply describes the extent to which the distribution is composed of the corresponding spherical harmonic. As in our earlier paper,[1] for the symbol $A_{q\pm}^{\{k\}}$ the brackets around the rank and the $+$ or $-$ after the component indicate that we are using the Hertel–Stoll notation[9] in which all the spherical tensors are real.

In Figs. 3 and 4 we show several examples of orientation data. Plotted is the integrated ion intensity vs the ellipticity angle β. As a check on our polarization optics and data reduction procedures, we have performed measurements on isotropic gas samples admitted to the chamber through a leak valve. These results are shown in Fig. 3(a) for the

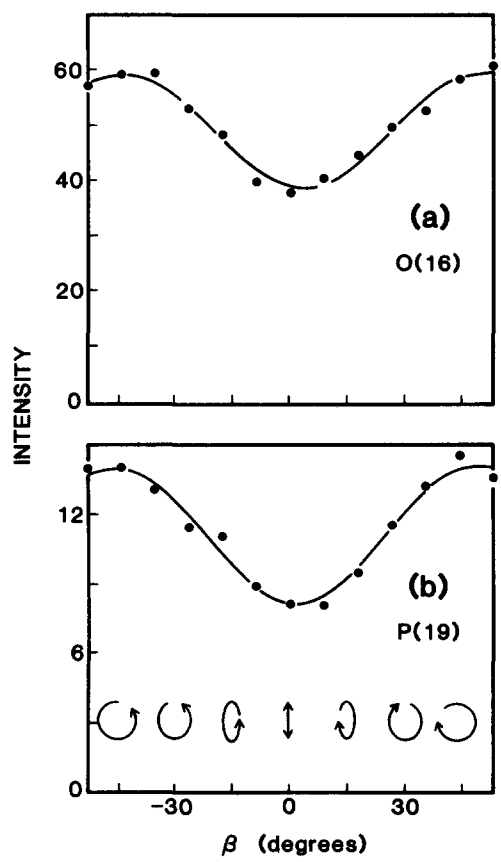

FIG. 3. Examples of orientation data for (a) $O(16)$ and (b) $P(19)$ for isotropic background gas recorded at a pressure of 2×10^{-7} Torr. Plotted is the integrated ion intensity as a function of β, the ellipticity of the laser polarization. $\beta = 0°$ corresponds to linear polarization, $\beta = \pm 45°$ to right or left circular polarization. The solid lines are fits to Eq. (1). The curves are symmetric about $\beta = 0°$ indicating no orientation.

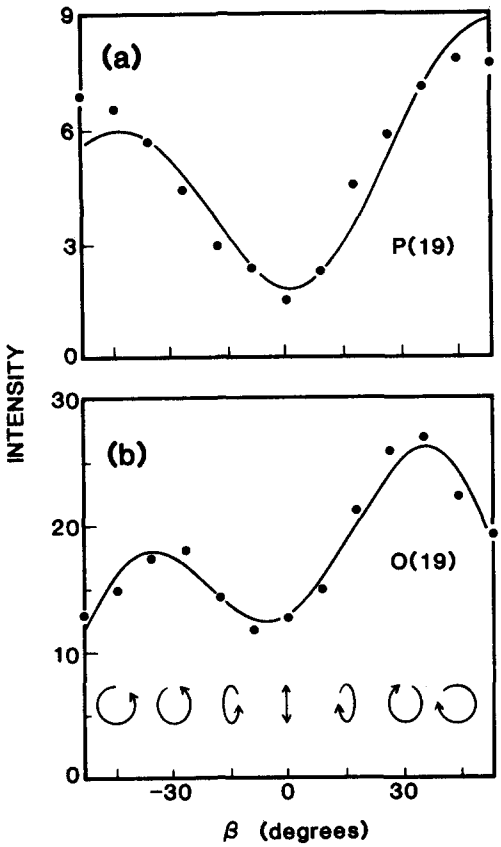

FIG. 4. Orientation data and fits for (a) $P(19)$ and (b) $O(19)$ for N_2 scattered off Ag(111). Conditions were $\theta_i = 30°$, $\theta_f = 35°$, $E_i = 0.3$ eV, and $T_s = 90$ K. The curves are asymmetric about $\beta = 0°$ indicating that the $J = 19$ level is oriented.

$O(16)$ and in Fig. 3(b) for the $P(19)$ lines of the N_2 $a\,^1\Pi_g - X\,^1\Sigma_g^+$ (1,0) band.

The integrated intensities as a function of β are fit in a least-squares manner to Eq. (1) to determine the moments. The solid curves shown in Figs. 3 and 4 are the fits. For the results presented in this paper, five terms were included in Eq. (1) to achieve a satisfactory fit: $A_{0+}^{\{0\}}$, $A_{0+}^{\{2\}}$, $A_{0+}^{\{4\}}$, $A_{1-}^{\{1\}}$, and $A_{1-}^{\{3\}}$. Qualitatively, we expect the surface normal to be a natural quantization axis for alignment because the dominant forces in the scattering lie in this direction. The $A_{0+}^{\{2\}}$ and $A_{0+}^{\{4\}}$ alignment moments have large amplitudes in the z direction and are therefore used in fitting the data. The $A_{1-}^{\{1\}}$ moment is the lowest order term describing orientation along y, i.e., along the direction toward which our measurement is sensitive. The $A_{1-}^{\{3\}}$ term must also be included because for large alignment of J perpendicular to z, it has the same form as $A_{1-}^{\{1\}}$. One additional orientation term could contribute, the $A_{3-}^{\{3\}}$ moment, but was found not to be needed to fit the data. This implies an upper limit of 0.10 for the value of this moment.

Explicit expressions for these terms are listed in Table I. A complete table of all the $A_{q\pm}^{\{k\}}$ for $k \leq 4$ and a discussion of how they could be measured are given in Ref. 8. The derived values of the polarization moments for Fig. 1 are for $J = 16$:

$$A_{0+}^{\{2\}} = 0.18(0.12), \quad A_{0+}^{\{4\}} = 0.11(0.12),$$

TABLE I. Expressions for the polarization moments measured in this work.

$$A_{0+}^{\{0\}} = 1$$

$$a_{0+}^{\{0\}} = n(J_i)C(\det)A_{0+}^{\{0\}} = n(J_i)C(\det)$$

$$A_{0+}^{\{2\}} = \langle(J_i|(3J_z2 - J^2)/J^2|J_i)\rangle$$

$$A_{0+}^{\{4\}} = (\tfrac{1}{8})\langle(J_i|)(3J^4 - 6J^2 - 30J_z2J^2 + 25J_{z^2} + 35J_{z^4})/(J^4)|J_i)\rangle$$

$$A_{1-}^{\{1\}} = \langle(J_i|J_y/J|J_i)\rangle$$

$$A_{1-}^{\{3\}} = [(\tfrac{3}{8})^{1/2}/4]\langle(J_i|(4J_{yz}2 - 3J_y3 - J_x2_y)/J^3|J_i)\rangle$$

$$A_{1-}^{\{1\}} = -0.016(0.011), \quad A_{1-}^{\{3\}} = -0.11(0.04),$$

and for $J = 19$:

$$A_{0+}^{\{2\}} = -0.38(0.45), \quad A_{0+}^{\{4\}} = 0.045(0.045),$$

$$A_{1-}^{\{1\}} = -0.019(0.024), \quad A_{1-}^{\{3\}} = -0.037(0.031).$$

The estimated error determined from the least-squares fit for each fitted parameter is given in parentheses and is one standard deviation. The data for isotropic gas were acquired at a pressure (2×10^{-7} Torr) chosen to yield signal levels comparable to those encountered in a scattering experiment. These results show essentially no orientation or alignment and can be used as a measure of our sensitivity to these parameters. These results also show that the circular to linear polarization ratio is 3:2, in agreement with previous calculations for two-photon excitation.[10]

It is a general feature of these orientation measurements that the fitted values of the alignment moments (those $A_{q\pm}^{\{k\}}$ with k even) are not very reliable because the corresponding line strengths vary little with ellipticity.[8] The fitted alignment values also depend critically on an accurate determination of the baseline in a wavelength scan and are very sensitive to small (10%) unresolved contributions from a line of another rotational branch. For these reasons, only the orientation moments are determined from data like that shown in Figs. 3 and 4. The alignment is much more accurately determined from a measurement where the direction of the polarization is varied for a fixed ellipticity. This we do for an infinite ellipticity, that is, for linearly polarized light, which has the added benefit of being completely insensitive to the orientation moments. The sample orientation is reflected only in the difference in intensity at $+\beta$ and $-\beta$ and is therefore insensitive to uncertainty in the base line position.

Figure 4 shows orientation data for N_2 specularly scattered from Ag(111) at $T_s = 90$ K for (a) $O(19)$ and for (b) $P(19)$. When data on two rotational branches are available for a given rotational level, the data are fit jointly to determine $A_{1-}^{\{1\}}$ and $A_{1-}^{\{3\}}$. This is of great utility because the $P_{1-}^{\{1\}}$ and $P_{1-}^{\{3\}}$ line strength terms have a very similar variation with β making differentiation between the two difficult if only one branch is resolved. However, the relative sign of the $P_{1-}^{\{1\}}$ and $P_{1-}^{\{3\}}$ contributions to the total line strength changes depending on whether ΔJ is ± 1 or ± 2. Thus, having data on two branches (commonly in our spectra of N_2 the O and P branches are well resolved) allows the $A_{1-}^{\{1\}}$ and $A_{1-}^{\{3\}}$ moment contributions to be readily separated. The

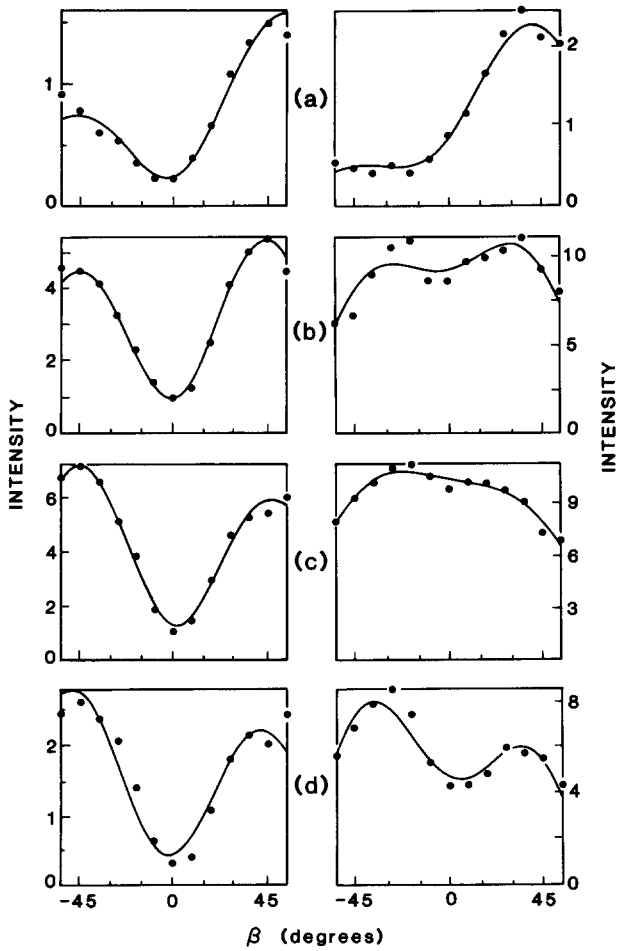

FIG. 5. Orientation data and fits for $O(18)$ (left set of figures) and $P(18)$ (right set) as a function of final scattering angle. Initial conditions were $\theta_i = 30°$, $E_i = 0.3$ eV, and $T_s = 90$ K. Final angles from the top of the page to the bottom were: $\theta_f = 25°$, $\theta_f = 35°$, $\theta_f = 45°$, and $\theta_f = 55°$ (all angles are measured with respect to the surface normal). It is seen that the orientation of the $J = 18$ level changes sign as the final angle is scanned from subspecular to superspecular.

values derived for the data in Fig. 4 are $A_{1-}^{\{1\}} = -0.26(0.05)$ and $A_{1-}^{\{3\}} = +0.22(0.10)$. Inspection of the form of the $A_{1-}^{\{1\}}$ and $A_{1-}^{\{3\}}$ moments shown in Table I indicates that for samples highly aligned with $\langle J_z \rangle$ near zero [the case for N_2 scattered from Ag(111)[1,2]] the ratio of these two terms should approach $-3/5$ (actually $-(3/8)^{1/2} \cong -0.61$). Therefore, in cases when only one branch is available and the alignment is measured to be large, the value of $A_{1-}^{\{3\}}$ is fixed at $-3/5 A_{1-}^{\{1\}}$ in fitting the orientation data.

IV. RESULTS AND DISCUSSION

The observation of nonzero values of the orientation moments indicates that the angular momentum of the scattered N_2 is oriented with respect to the laser propagation direction. This is illustrated in cartoon form in Fig. 1, which also shows the relation between the sign of the moments and sense of rotation. As depicted, $A_{1-}^{\{1\}}$ greater than zero implies that **J** preferentially points in the same direction as the laser. A perfectly oriented sample, i.e., one in which all the population is in $J_y = +J$ (or $J_y = -J$) would have $A_{1-}^{\{1\}} = +1$ (or -1) and $A_{1-}^{\{3\}} = -3/5$ (or $+3/5$).

The observed orientation is found to depend strongly in both magnitude and sign on the direction that the molecule leaves the surface. Results are shown in Fig. 5 for $J = 18$ as a function of detection angle. The data in the left set of figures is for $O(18)$; the right set is for $P(18)$. Final scattering angles are: (a) $\theta_f = 25°$ (b) 35°, (c) 45°, and (d) 55°. The sense of rotation changes as the final angle is changed from subspecular to superspecular indicating a strong correlation between orientation and scattering geometry. We have performed a series of measurements to determine alignment, orientation, and population for three different final angles as a function of rotational quantum number. The results are shown in Figs. 6–8. All the data were recorded with the surface held at 90 K, incident angle at 30°, and incident energy at 0.3 eV. In panels (a) and (d) of Figs. 6 and 7, and panel (a) of Fig. 8, the laser focus is positioned at an angle of 20° with respect to the surface normal (we will call this the subspecular angle); in panels (b) and (e) of Figs. 6 and 7, and panel (b) of Fig. 8 the focus is at 35° (termed the specular angle), and in panels (c) and (f) of Figs. 6 and 7 and panel (c) of Fig. 8 the laser focus is at 50° (termed the superspecular angle). As discussed in Ref. 1, the combination of molecular beam spot size on the crystal and crystal to laser focus distance yield an angular acceptance of $\sim 15°$. Thus, our results represent a convolution of the true angular distribution and an instrument function related to the geometry of our apparatus. We will not attempt to deconvolute the data for the instrument function.

A. Alignment

The quadrupole ($A_{0+}^{\{2\}}$) and hexadecapole ($A_{0+}^{\{4\}}$) alignment have been measured as a function of rotational quantum number for the three final angles mentioned above (subspecular, specular and superspecular). Results are shown in Fig. 6. The limiting values for the alignment moments are: $A_{0+}^{\{2\}} = -1.0$ for **J** perpendicular to $\hat{\mathbf{n}}$ and $A_{0+}^{\{2\}} = +2$ for **J** parallel to $\hat{\mathbf{n}}$, where $\hat{\mathbf{n}}$ is the surface normal; for the hexadecapole moment: $A_{0+}^{\{4\}} = +0.375$ (**J** perpendicular to $\hat{\mathbf{n}}$), $A_{0+}^{\{4\}} = +0.75$ (**J** parallel to $\hat{\mathbf{n}}$), and $A_{0+}^{\{4\}} = -0.50$ (**J** at an angle of 49° to $\hat{\mathbf{n}}$). At high J the scattered N_2 is seen to be very highly aligned with **J** perpendicular to $\hat{\mathbf{n}}$, which agrees with our previous results.[1,2,7] Interpretation of the value of the $A_{0+}^{\{4\}}$ moment may require knowing the $A_{0+}^{\{2\}}$ moment first because the $A_{0+}^{\{4\}}$ moment has two regions of positive sign. In most cases, we derive a large negative quadrupole moment (**J** perpendicular to $\hat{\mathbf{n}}$) and the measured hexadecapole alignment in the range of 0.1–0.38 reinforces the conclusion that **J** is highly aligned perpendicular to $\hat{\mathbf{n}}$.

For the specular alignment data shown in Fig. 6(b) and 6(e), we observe the degree of alignment to increase with rotational quantum number J: the alignment is small for low J values ($1 < J < 4$) and increases smoothly with J, approaching at high J the limiting values for **J** pointing perpendicular to $\hat{\mathbf{n}}$.

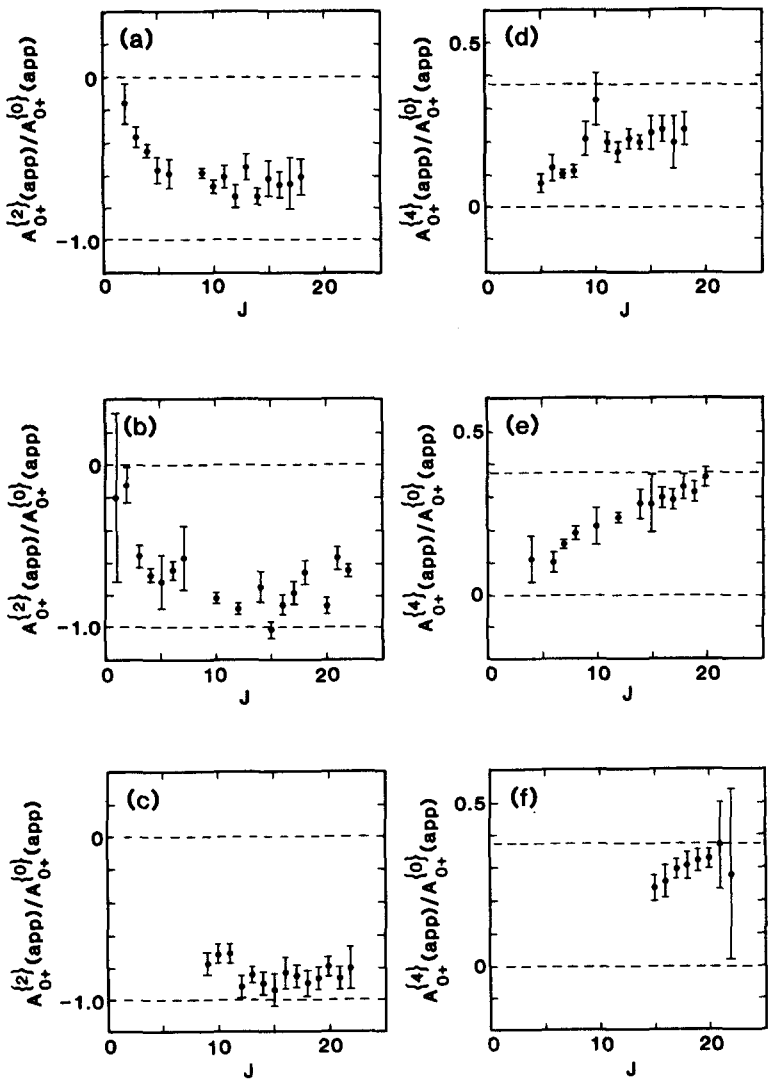

FIG. 6. Quadrupole $A_{0+}^{\{2\}}$ and hexadecapole $A_{0+}^{\{4\}}$ alignment moments as a function of rotational quantum number for subspecular ($\theta_f = 25°$, top panels), specular ($\theta_f = 35°$, middle panels) and superspecular ($\theta_f = 50°$, bottom panels). The incident conditions were $\theta_i = 30°$, $E_i = 0.3$ eV, and $T_s = 90$ K.

At the superspecular angle, the alignment is found to be the same as at specular, within our error bars. We do not have values for the alignment for J values less than eight at superspecular because the line intensities are too low in these levels (see Fig. 9 for the populations).

For the subspecular angle, the trend in the alignment is the same as for specular, but the limiting value of $A_{0+}^{\{2\}} \cong -0.70$ at J values greater than ten for the quadrupole moment is significantly less than at the specular angle $[A_{0+}^{\{2\}}(J>10) \cong -0.85]$. We offer a possible explanation of this in the next section. The hexadecapole moment is also less at the subspecular angle than at specular, although the difference is less obvious than the difference in the $A_{0+}^{\{2\}}$ moment.

B. Orientation

The dipole ($A_{1-}^{\{1\}}$) and octupole ($A_{1-}^{\{3\}}$) orientation moments are presented in Fig. 7 as a function of J for the three final scattering angles. A nonzero value for these moments indicates a preference for **J** to point preferentially along or against the laser propagation direction. As noted earlier, the value of the $A_{1-}^{\{1\}}$ moment can range from $+1$ to -1; $A_{1-}^{\{1\}} = +1$ corresponds to **J** pointing in the same direction as the laser beam propagates, and $A_{1-}^{\{1\}} = -1$ the opposite (see Fig. 1). The $A_{1-}^{\{3\}}$ octupole moment contains additional information relating to the projection of **J** onto the **z** axis. For samples that are highly aligned with **J** perpendicular to $\hat{\mathbf{n}}$, which is along **z**, $A_{1-}^{\{3\}}$ assumes a fixed relationship to $A_{1-}^{\{1\}}$ (see Table I). Since $A_{1-}^{\{1\}}$ is directly proportional to $\langle J_y/\mathbf{J} \rangle$, the magnitude of the $A_{1-}^{\{1\}}$ moment can be roughly interpreted as the fractional difference in the population of molecules in states with $+J_y$ and $-J_y$. Thus $A_{1-}^{\{1\}} = -0.5$ means that approximately 75% of the molecules have **J** in the $-$**y** half-space. Similarly, $A_{1-}^{\{1\}} = -0.25$ implies that $\sim$62% of the sample has **J** along $-$**y**.

The deconvolution procedure used to extract the alignment moments at low J does not work as well when applied to orientation data. Commonly, the higher rotational levels are more oriented than the lower levels in the blended feature so that a small $+\beta/-\beta$ difference in ion intensity for the low J is masked by a relatively large difference arising from the underlying oriented high J. This makes the subtraction

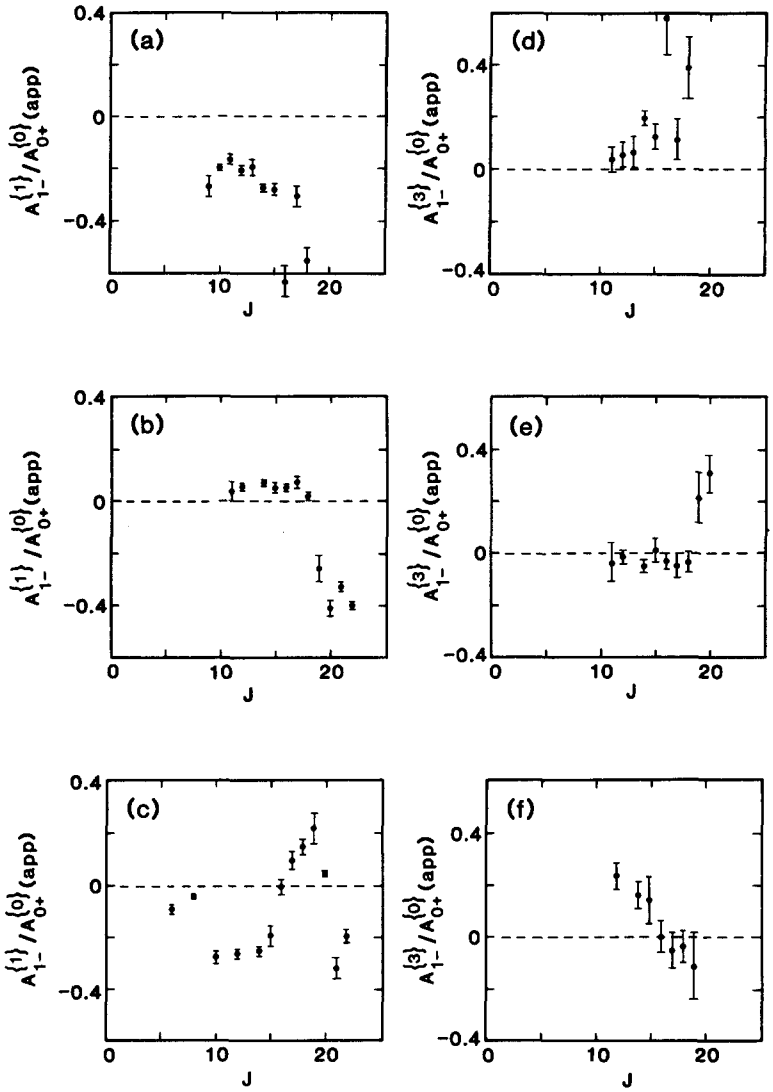

FIG. 7. Dipole $A_{1-}^{\{1\}}$ and octupole $A_{1-}^{\{3\}}$ orientation moments as a function of rotational quantum number for subspecular ($\theta_f = 25°$, top panels), specular ($\theta_f = 35°$, middle panels) and superspecular ($\theta_f = 50°$, bottom panels). The incident conditions were $\theta_i = 30°$, $E_i = 0.3$ eV, and $T_s = 90$ K.

procedure unreliable, and for the orientation results we present data only for unblended lines.

For scattering at specular, we observe a small positive orientation ($A_{1-}^{\{1\}} \sim +0.05$) for J values of 7 to 17. For J greater than 17, the orientation jumps to $A_{1-}^{\{1\}} \sim -0.50$. The trend for the $A_{1-}^{\{3\}}$ moment mirrors that of the $A_{1-}^{\{1\}}$, i.e., it is near zero for $7 < J < 17$ and then jumps abruptly to large values ($\sim +0.30$) for J greater than 17. The ratio $A_{1-}^{\{1\}}/A_{1-}^{\{3\}}$ at high J is $\sim -0.5/0.3 = -5/3$ as expected for a sample aligned with $\langle J_z \rangle \sim 0$. This result is consistent with the alignment data presented in Fig. 6 where it was shown that $\langle J_z \rangle$ was near zero.

The orientation moments at the subspecular angle are shown in Figs. 7(a) and 7(d). The dipole orientation is negative at all J values observed ($9 \leqslant J \leqslant 18$) and again shows a sharp jump at the highest J value. The subspecular results do not follow as well the $A_{1-}^{\{1\}}/A_{1-}^{\{3\}}$ ratio of 5 to 3 as the specular results. This is consistent with the significantly smaller alignment observed at this angle [see Figs. 6(a) and 6(d)]. For both the specular and subspecular data, the jump in orientation around $J = 18$ is not correlated with a change in the alignment at this level. This is some indication that the breakdown in cylindrical symmetry associated with nonzero orientation is not reflected by a concurrent change in the values of the noncylindrically symmetric alignment moments. As discussed in detail in Ref. 1, the alignment moments are apparent moments and include contributions from noncylindrically symmetric moments, i.e., terms like $A_{2+}^{\{2\}}$ and $A_{2+}^{\{4\}}$. If the magnitude of the contributions of these noncylindrically symmetric alignment moments were to change substantially around $J = 18$, we would expect to see a corresponding change in the values of the $A_{0+}^{\{2\}}$ (app) and $A_{0+}^{\{4\}}$ (app) moments.

The situation at the superspecular angle is more complicated. The dipole orientation moment shows striking structure with J, changing sign from negative to positive at $J = 16$ and again turning negative above $J = 20$. The $A_{1-}^{\{1\}}/A_{1-}^{\{3\}}$ ratio follows very closely the $-5/3$ high-alignment ratio for all levels where we can determine both. As seen in the subspecular data, the structure in the superspecular orientation moments is not well correlated with variations in the alignment.

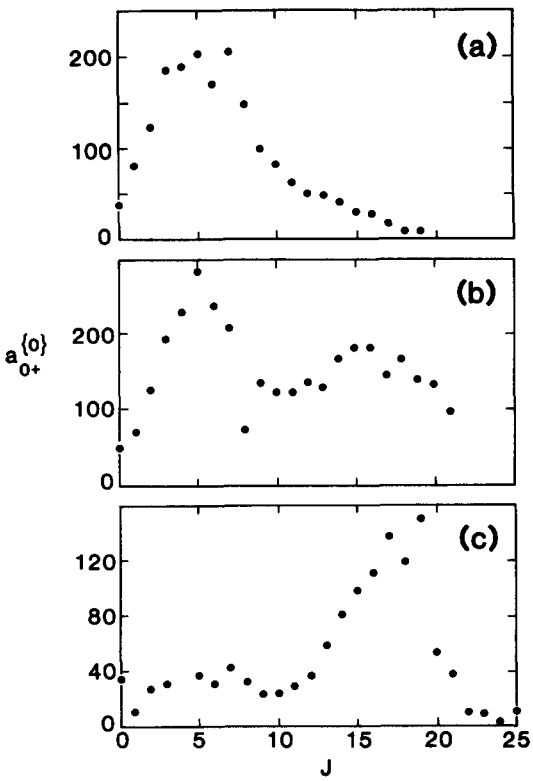

FIG. 8. Rotational state populations, $a_{0+}^{\{0\}}$, as a function of rotational quantum number for (a) subspecular ($\theta_f = 25°$); (b) specular ($\theta_f = 35°$); and (c) superspecular ($\theta_f = 50°$). The incident conditions were $\theta_i = 30°$, $E_i = 0.3$ eV, and $T_s = 90$ K. Plotted is the population divided only by the nuclear spin degeneracies (but not the rotational degeneracies).

C. Populations

The rotational state populations as a function of J for the three final angles are shown in Fig. 8. The data are plotted showing $n(J)$ as a function of J, i.e., the plot shows the actual relative populations of the J levels, corrected only for the nuclear spin degeneracy (but not for the rotational degeneracy). The individual plots are not normalized. Instead, the curves at each angle are scaled relative to one another according to the total population defined as

$$n = \sum A_{0+}^{\{0\}}(J).$$

These results have been presented previously[1] in the form of Boltzmann plots; here we replot the data in a different form to facilitate comparison to the orientation data.

The results in Fig. 8 show a strong shift of population to higher J levels as the final angle is probed further from the surface normal. This has been discussed in some detail before,[1,11] as has the origin of the rotational rainbow seen in Figs. 8(b) and 8(c),[11,12] and will not be repeated here.

The remarkable variation with final scattering angle observed for the orientation is also evident in the J state distributions. In addition, the structure in the orientation as a function of J is correlated with the position of the rainbow in the population distribution. This is particularly noticeable for the data taken at the superspecular angle. The negative dip in the orientation for J values of 10 to 14 is mirrored by a local minimum in the population for these levels; the positive-going bump in the orientation for J values of 16–20 correlates with the rainbow peak in the population, and the rapid negative drop in orientation for J greater than 18 is accompanied by the population falloff above the rainbow maximum. The specular orientation data also show a rapid negative drop in orientation for J greater than the rainbow $J(J_R \sim 18)$. These correlations between the observed orientation and the rotational rainbow will be explored in Sec. V.

V. FRICTIONAL HARD-CORE HARD-ELLIPSOID MODEL

The results of Sec. IV demonstrate that significant net orientation of rotational angular momentum is produced in collisions of nitrogen molecules with a Ag(111) surface. Furthermore, there is a complicated dependence of the orientation on parameters such as final scattering angle and final rotational state. The molecules do not simply develop a small amount of "topspin" on impact. Indeed, under some conditions molecules excited to intermediate final rotational states, on average, are rotating in a counterintuitive "backwards" sense; i.e., they develop a net "backspin" rather than topspin.

In this section we discuss the physical origin of this behavior, aided by a simple "frictional hard-cube hard-ellipsoid model." The model is sufficient to reproduce at least qualitatively all of the trends in rotational orientation observed experimentally. In a separate paper[16] we will present detailed comparisons between the experimental results reported here and three-dimensional stochastic trajectory calculations invoking moving surface atoms and realistic interaction potentials.

The model we propose is a simple extension of the hard-cube models that have been applied extensively in the analysis of atomic and molecular scattering from smooth surfaces.[13] Without tangential forces of some kind, however, there can be no net orientation in the rotation of the scattered ellipsoid. We introduce tangential forces into the model in a simple way, namely by the addition of a frictional force directed parallel to the surface that acts on the ellipse at its point of contact with the cube and is proportional to the initial tangential component of velocity of the ellipse, v_x. This is consistent with the desired physical picture of a ball picking up topspin. The model is illustrated in Fig. 9 and presented in the Appendix.

The representation of tangential forces as a frictional force in this model does not require that the actual tangential forces acting on the molecule are dissipative. Scattering of a molecule from a rigid surface with a corrugated gas–surface interaction potential can produce angular momentum orientation because the net laterally averaged force will be in the direction opposing the lateral velocity. This nondissipative mechanism can be represented by the frictional force in our model. Alternative dissipative mechanisms for producing tangential forces, such as creation of tangentially directed phonons or electron–hole pairs, could also contribute to the observations and can also be represented by the frictional term in our model.

Consider first the predictions of the model for $T_s = 0$

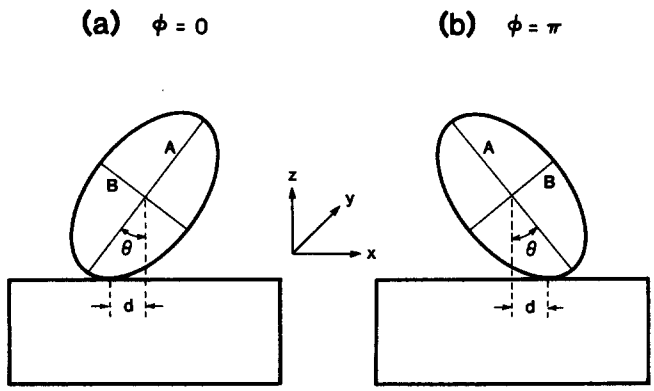

FIG. 9. Illustration of the frictional cube model. A and B are, respectively, the ellipse major and minor axes, and d is the moment arm at the instant of impact. Cases (a) and (b) show the impact angles leading to maximum rotational excitation. In the absence of inplane forces, the two situations lead to the same rotational excitation. Inclusion of inplane forces results in different amounts of rotational excitation for the two cases.

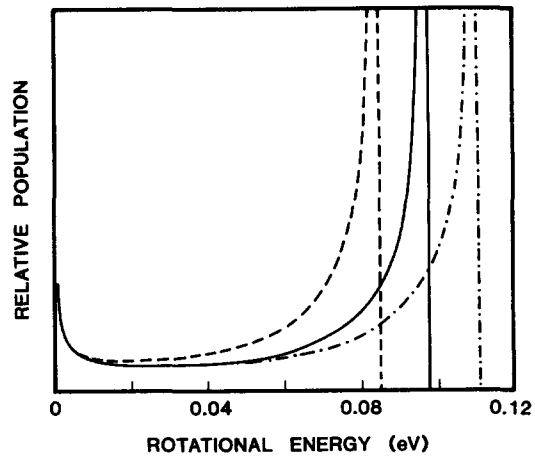

FIG. 10. Rotational energy distributions calculated from the frictional cube model. The solid curve is for the case of no in-plane forces, the broken curves are for cases (a) (dot–dash) and (b) (dashed only) of Fig. 9, and include an in-plane force.

and $\gamma = 0$ (no tangential friction). For an incident translational energy of 0.3 eV and incident angle of 30°, the rotational energy distribution computed by the model is given by the solid curve of Fig. 10. The distribution exhibits a strong rainbow singularity at $E_R = 0.098$ eV. The rainbow feature is a singularity in this simple classical mechanical model, with no tangential friction, because we have assumed a smooth structureless surface and have taken the initial surface and rotational temperatures to be zero. In a more realistic calculation the rainbow feature will be rounded because of averaging over impact sites on a corrugated surface, thermal motion of the surface atoms, and initial rotational motion of the molecule.[14,15] Quantum broadening may also contribute, particularly for light molecules. In spite of all these mechanisms acting to wash out the rainbow, a distinct, albeit smooth, feature is observed experimentally.

The presence of the rainbow feature is critical to the rotational orientation behavior reported in Sec. IV. We now examine the predictions of the simple model with all parameters identical to the above example, except that the dimensionless lateral friction parameter γ is now taken to be 0.16. Let us first average, as before, over initial molecular axis direction θ according to Eq. (A11), but constrain the initial aximuthal angle ϕ to be zero. Thus, the major axis of the ellipse will lie in the collision plane, and the ellipse will be tilted forward at the instant of impact as illustrated in Fig. 9(a). For this geometry, the component of momentum J_y' imparted by forces perpendicular to the smooth surface, the usual and dominant source of angular momentum, is negative. The smaller additional contribution to J_y' from tangential friction is also negative (topspin), so the two contributions add to give higher total $|J_y'|$ and thereby push the rainbow associated with this class of constrained geometries to higher E_R (dot–dash curve of Fig. 10). Thus, J_y' will be strongly negative for the highest values of E_R, as observed experimentally.

In contrast, consider collisions constrained so that $\phi = \pi$; i.e., the ellipse is initially tilted back as in Fig. 9(b). For this geometry, the dominant impulsive forces will produce positive J_y' (backspin). Subtraction of the negative contribution from tangential friction will thus produce a smaller maximum $|J_y'|$ for this class of geometries, pushing the rainbow to lower E_R (dashed curve of Fig. 10). The sign of J_y' remains positive for collisions of this geometry. Thus the addition of tangential friction splits the rainbow, with the lower energy portion displaying positive J_y' and the high energy part negative J_y'. In the region of the lower energy part of the rainbow, a net backspin, $J_y' > 0$ will be created, as observed experimentally. The backspin is not a consequence of any special kind of trajectory (e.g., double hits) or of quantum effects but rather results from the distribution of ordinary trajectories in the vicinity of the rotational rainbow.

The above discussion is oversimplified. The azimuthal angle is, of course, not constrained to be either 0 or π but is distributed uniformly between 0 and 2π. Thus, a double rainbow singularity as suggested in Fig. 10 is not observed. Instead, the distribution fills in the region between the two extremes of Fig. 10, and the rainbow singularity is removed. Based on the experimental results of Sec. IV, tangential friction (in-plane forces) is a major contribution to rounding the rainbow.

As shown in Fig. 11, averaging over all ϕ does not destroy the correlation of J_y' with E_R. The highest E_R molecules exhibit strong topspin, and those of intermediate E_R in the vicinity of the $\phi = \pi$ rainbow show a net backspin and positive J_y'. The average value of J_y' integrated over all E_R is -0.031 confirming the net topspin influence or the applied tangential friction. Thus, the simple frictional hard-cube hard-ellipsoid model demonstrates how a tangential friction that is responsible for a small average rotational orientation can produce very large orientation of the opposite sign at certain values of J caused by the focusing effects of the rotational rainbow.

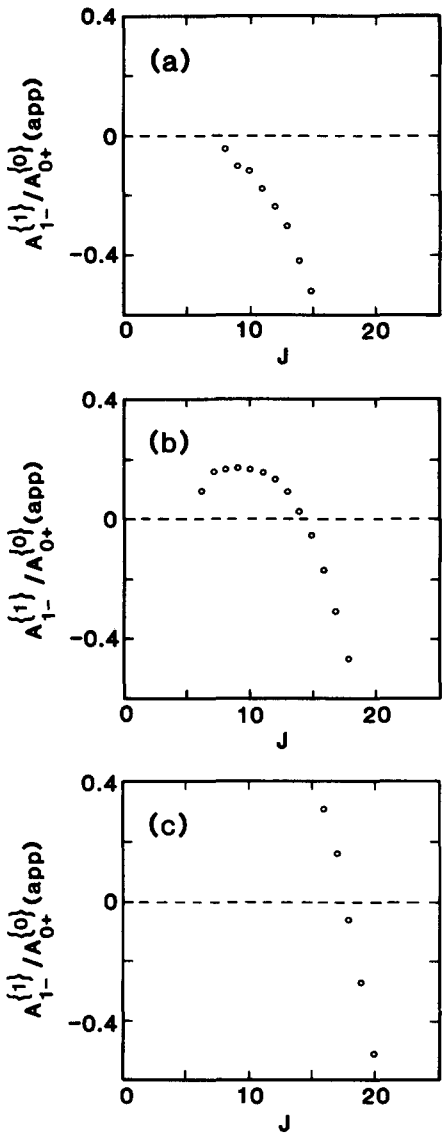

FIG. 11. Dipole orientation moments calculated from the frictional cube model for three different final scattering angles.

VI. CONCLUSIONS

We have observed rotational orientation in the scattering of N_2 from clean Ag(111). The orientation is large, can be of either the intuitive or counterintuitive sign, and exhibits an interesting dependence on final angular momentum and scattering angle. The major experimental features can be reproduced qualitatively by the simple hard-cube hard-ellipsoid model to which a tangential frictional force has been added to represent the laterally averaged in-plane surface forces. The striking changes of sign of orientation result from a splitting of the rotational rainbow by in-plane forces. Indeed, the presence, location, and degree of smearing of the rainbow are revealed dramatically in the orientation measurements, in contrast to total angular momentum distributions that typically exhibit only a modest shoulder.

The origin of the tangential forces in the N_2–Ag(111) system is the weak but nonzero corrugation of the interaction potential. Excitation of electron–hole pairs could contribute, in principle, but it is unlikely that this mechanism is significant at the low incident velocities studied here, as supported by the ability of stochastic trajectory calculations to reproduce the results without invoking an electronic mechanism. Corrugation induced by thermal fluctuations is also not a dominant factor, as shown by experiments to be reported elsewhere[16]: The measured orientation decreases with increasing surface temperature. Tangential forces that are dissipative (phonon creation) or nondissipative (rigid deflection) probably both contribute to the creation of orientation. However, short-wavelength corrugations are required, in contrast to the nature of corrugations that influence angular distributions. Any surface region of small or large area with a local normal that is tilted with respect to the overall surface normal will affect the angular scattering distribution. But simply tilting a flat region produces no rotational orientation (excluding effects due to the edge of the region). Corrugations of wavelength comparable to the spatial extent of the molecule are required. Thus, rotational orientation reveals a different aspect of surface corrugation than angular distributions or energy barriers to diffusion, thereby offering independent and valuable information about gas–surface interaction potentials.

The strong orientational polarization we have measured is for a system that might have been expected to exhibit only a small effect. N_2 is a weakly aspherical molecule, as judged by its charge contours. In addition, Ag(111) is a very flat, smooth surface, and N_2 binds weakly to it. Molecules which are more highly asymmetric and which exhibit strong directional bonding to surfaces may exhibit even more striking rotational orientation. Corrugated or stepped surfaces may further enhance orientation. Thus, rotational orientation may provide a useful and general probe of in-plane gas–surface forces.

ACKNOWLEDGMENTS

This work was supported by the Office of Naval Research under Grant No. N00014-87-K-0265.

APPENDIX

We develop the hard-cube hard-ellipsoid model for a homonuclear diatomic molecule scattering from a solid surface. Referring to Fig. 9, the response of the surface is represented by a cube of effective mass M. The cube is constrained to move in the z (surface normal) direction only, with initial velocity u_z at the instant prior to the collision distributed according to a Boltzmann distribution at the surface temperature T_s. The gas molecule is represented by a hard ellipsoid of mass m, and moment of inertia I, with major and minor axes A and B, respectively. The center of mass of the ellipsoid moves in the x–z plane with components of velocity prior to collision given by v_x and v_z. The ellipsoid is assumed to be initially not rotating. The moment arm at the instant of impact is denoted by d (see Fig. 9).

For a given set of initial ellipsoid velocity components v_x and v_z, initial cube speed u_z, and initial polar and azimuthal angles θ and ϕ defining the direction of the major

axis of the ellipsoid relative to the surface normal, the final velocity components and angular momenta are given by

$$v_x' = (1-\gamma)v_x, \tag{A1}$$

$$v_y' = v_y = 0, \tag{A2}$$

$$v_z' = v_z - \frac{2(v_z - u_z)}{md^2/I + m/\mu}, \tag{A3}$$

$$J_x' = \frac{2(v_z - u_z)d\sin\phi}{d^2/I + 1/\mu}, \tag{A4}$$

$$J_y' = -\frac{2(v_z - u_z)d\cos\phi}{d^2/I + 1/\mu} + \frac{1}{2}\gamma mRv_x\cos\theta, \tag{A5}$$

$$J_z' = \tfrac{1}{2}\gamma mRv_x\sin\theta\sin\phi, \tag{A6}$$

$$|J'| = [J_x'^2 + J_y'^2 + J_z'^2]^{1/2}. \tag{A7}$$

The molecule–surface reduced mass μ is defined by

$$\mu = \frac{mM}{m+M}, \tag{A8}$$

and d is the moment arm as defined in Fig. 9 and γ is the dimensionless tangential friction parameter. If the friction parameter is chosen to be zero, then Eqs. (A1)–(A6) are the usual hard-ellipsoid, hard-cube equations and can be easily derived from conservation of total energy, linear momentum and angular momentum. In this $\gamma = 0$ limit, nonzero angular momentum components J_x and J_y can be produced in individual collisions. However, the initial aximuthal angle ϕ is distributed randomly over the interval 0 to 2π so that the average values of J_x' and J_y', as well as J_z', must be identically zero.

The introduction of a tangential friction has two effects. First, it modifies the center-of-mass velocity in the x direction according to Eq. (A1). Second, it produces an additional contribution to the angular momentum $\mathbf{J}^{(f)}$ which we require to be the cross product,

$$\mathbf{J}^{(f)} = \gamma m\mathbf{v}^{(f)}x\frac{\mathbf{R}}{2}, \tag{A9}$$

where $\mathbf{v}^{(f)} = v_x$ is the initial molecular velocity in the x direction and $\mathbf{R}$ is the internuclear axis vector. The second term on the right-hand side of Eq. (A5) need not average to zero. Thus, a net nonzero orientation $\langle J_y' \rangle$ can be produced along the y direction (into the page in Fig. 10). The net orientation along the x and z directions must still vanish.

Equations (A1)–(A6) determine the final components of velocity and angular momentum for a particular set of initial parameters. Under the conditions reported here, the initial scattering direction and speed are fixed: i.e., v_x and v_z are the same for all trajectories. The moment arm d is determined by the initial bond direction:

$$d = \frac{(A^2 - B^2)\cos\theta\sin\phi}{2[A^2\cos^2\theta + B^2\sin^2\theta]^{1/2}}. \tag{A10}$$

The initial bond direction is random: i.e., the distributions of polar and azimuthal angles θ and ϕ are

$$P(\theta)d\theta = \sin\theta d\theta, \quad 0 < \theta < \pi/2, \tag{A11}$$

$$P(\phi)d\phi = \frac{1}{2\pi}d\phi, \quad 0 < \phi < 2\pi. \tag{A12}$$

Finally, the cube velocity u_z is distributed according to a Boltzmann distribution at the surface temperature T_s. As shown elsewhere,[17] the distribution of u_z, at the instant of impact is thus

$$P(u_z)du_z = \left[\frac{m}{2\pi k_B T_s}\right]^{1/2} \times\frac{(v_z - u_z)}{v_z}\exp\left[\frac{-Mu_z^2}{2k_B T_s}\right]du_z, u_z > -|v_z|, \tag{A13}$$

where k_B is Boltzmann's constant.

Numerical calculation of the averaged properties prescribed by the model is straightforward. Initial values of θ, ϕ, and u_z are chosen from uniform distributions in the appropriate ranges, and the final properties calculated from Eqs. (A1) to (A7), using Eq. (A10). The final values are weighted by the product of the distribution functions, Eqs. (A11) to (A13). For all the model calculations we have taken $m = 28$ amu (nitrogen molecule), $M = 431$ amu (four silver atoms), $A = 3.07$ Å, $B = 2.20$ Å, and $I = 8.434$ amu Å^2 (nitrogen molecule).

[1] G. O. Sitz, A. C. Kummel, and R. N. Zare, J. Chem. Phys. **89**, 2558 (1988).
[2] G. O. Sitz, A. C. Kummel, and R. N. Zare, J. Chem. Phys. **87**, 3247 (1987).
[3] L. J. F. Hermans, J. J. G. M. van der Tol, and J. J. M. Beenakker, J. Chem. Phys. **84**, 1029 (1986).
[4] L. V. Novakoski and G. M. McClelland, Phys. Rev. Lett. **59**, 1259 (1987).
[5] P. R. Brooks, Science **193**, 11 (1976); R. D. Levine and R. B. Berstein, *Molecular Reaction Dynamics and Chemical Reactivity* (Oxford University, Oxford, 1987).
[6] T. R. Proctor, D. J. Kouri, and R. B. Gerber, J. Chem. Phys. **80**, 3845 (1984).
[7] A. C. Kummel, G. O. Sitz, and R. N. Zare, J. Chem. Phys. **85**, 6874 (1986).
[8] A. C. Kummel, G. O. Sitz, and R. N. Zare, J. Chem. Phys. **88**, 6707 (1988).
[9] I. V. Hertel and W. Stoll, Adv. At. Mol. Phys. **13**, 113 (1978).
[10] R. B. Bray and R. M. Hochstrasser, Mol. Phys. **31**, 1199 (1976); J. B. Halpern, H. Zacharias, and R. Wallenstein, J. Mol. Spectrosc. **79**, 1 (1980); K. M. Chen and E. S. Young, J. Chem. Phys. **69**, 43 (1978).
[11] R. Schinke, J. Chem. Phys. **76**, 2352 (1982).
[12] A. W. Kleyn, A. C. Luntz, and D. J. Auerbach, Phys. Rev. Lett. **47**, 1169 (1981).
[13] W. L. Nichols and J. H. Weare, J. Chem. Phys. **62**, 3754 (1975); **63**, 379 (1975); **66**, 1075 (1977); J. A. Barker and D. J. Auerbach, Chem. Phys. Lett. **67**, 393 (1979); G. D. Kubiak, J. E. Hurst, Jr., H. G. Rennagel, G. M. McClelland, and R. N. Zare, J. Chem. Phys. **79**, 5163 (1983).
[14] J. E. Hurst, Jr., G. D. Kubiak, and R. N. Zare, Chem. Phys. Lett. **93**, 235 (1982).
[15] C. W. Muhlhausen, L. R. Ruby, and J. C. Tully, J. Chem. Phys. **83**, 2594 (1985).
[16] A. C. Kummel, G. O. Sitz, R. N. Zare, and J. C. Tully (in preparation).
[17] E. K. Grimmelmann, J. C. Tully, and M. J. Cardillo, J. Chem. Phys. **72**, 1039 (1980).